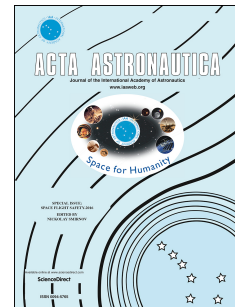


Accepted Manuscript

Validation of vibration-dissociation coupling models in hypersonic non-equilibrium separated flows

G. Shoev, G. Oblapenko, O. Kunova, M. Mekhonoshina, E. Kustova



PII: S0094-5765(17)31298-5

DOI: [10.1016/j.actaastro.2017.12.023](https://doi.org/10.1016/j.actaastro.2017.12.023)

Reference: AA 6603

To appear in: *Acta Astronautica*

Received Date: 15 September 2017

Revised Date: 13 November 2017

Accepted Date: 15 December 2017

Please cite this article as: G. Shoev, G. Oblapenko, O. Kunova, M. Mekhonoshina, E. Kustova, Validation of vibration-dissociation coupling models in hypersonic non-equilibrium separated flows, *Acta Astronautica* (2018), doi: [10.1016/j.actaastro.2017.12.023](https://doi.org/10.1016/j.actaastro.2017.12.023).

This is a PDF file of an unedited manuscript that has been accepted for publication. As a service to our customers we are providing this early version of the manuscript. The manuscript will undergo copyediting, typesetting, and review of the resulting proof before it is published in its final form. Please note that during the production process errors may be discovered which could affect the content, and all legal disclaimers that apply to the journal pertain.

Validation of vibration-dissociation coupling models in hypersonic non-equilibrium separated flows

G. Shoev^{a,b,c}, G. Oblapenko^{b,*}, O. Kunova^b, M. Mekhonoshina^b, E. Kustova^b

^a*Novosibirsk State University, 2 Pirogova str., Novosibirsk 630090, Russia*

^b*Saint Petersburg State University, 7/9 Universitetskaya nab., St. Petersburg, 199034, Russia*

^c*Khristianovich Institute of Theoretical and Applied Mechanics, Institutskaya 4/1, Novosibirsk 630090, Russia*

Abstract

The validation of recently developed models of vibration-dissociation coupling is discussed in application to numerical solutions of the Navier–Stokes equations in a two-temperature approximation for a binary N₂/N flow. Vibrational-translational relaxation rates are computed using the Landau–Teller formula generalized for strongly non-equilibrium flows obtained in the framework of the Chapman–Enskog method. Dissociation rates are calculated using the modified Treanor–Marrone model taking into account the dependence of the model parameter on the vibrational state. The solutions are compared to those obtained using traditional Landau–Teller and Treanor–Marrone models, and it is shown that for high-enthalpy flows, the traditional and recently developed models can give significantly different results. The computed heat flux and pressure on the surface of a double cone are in a good agreement with experimental data available in the literature on low-enthalpy flow with strong thermal non-equilibrium. The computed heat flux on a double wedge qualitatively agrees with available data for high-enthalpy non-equilibrium flows. Different contributions to the heat flux calculated using rigorous kinetic theory methods are evaluated. Quantitative discrepancy of numerical and experimental data is discussed.

Keywords: multi-temperature, high enthalpy, separated flows, vibration-dissociation coupling

1. Introduction

Under cruising conditions and during maneuvering in super- and hypersonic flights, shock waves arise near air vehicles. Depending on the free-stream parameters and the construction of the flying craft these shock waves can intersect

*Corresponding author

Email addresses: gerashoev@yandex.ru (G. Shoev), kunstmord@kunstmord.com
(G. Oblapenko), kunova.olga@gmail.com (O. Kunova), mekhonoshinama@gmail.com
(M. Mekhonoshina), e.kustova@spbu.ru (E. Kustova)

near certain elements of its construction. Interference of shock waves and their interaction with the boundary layer can lead to flow separation, and consequently to drastic changes in integral and distributed surface characteristics of the air vehicle. Correct prediction of surface characteristics (such as the heat flux) of flying crafts is vitally important for optimizing their construction.

Behind strong shock waves occurring during atmospheric re-entry (SHEFEX [1, 2], IXV [3], etc.), various physical processes occur. Vibrational modes of molecules are excited, dissociation and ionization reactions take place, heat is transferred via radiation, and can be significantly affected by the catalytic activity on the surface of the spacecraft. Correct mathematical description of these processes should provide accurate and reliable prediction of surface characteristics, in particular, heat loads, which are needed for development of thermal protection systems for re-entry vehicles.

Two of the key processes, significantly influencing results of numerical modeling, are vibrational-translational (VT) relaxation and dissociation. Due to progress in computational performance, lately, attention has been directed towards validation of mathematical models for description of these processes.

A detailed comparison between computation results and experimental measurements of vibrational temperature of oxygen for flows behind shock waves is presented in multiple works [4, 5, 6, 7, 8]. Comparisons of results of numerical modeling of electron density near a capsule during atmospheric re-entry with orbital velocity with experimental data obtained via reflectometers can be found in [9, 10, 11, 12]. Validation of various models of VT relaxation and dissociation has been performed by comparing computed [13] and experimentally [14] measured shock standoff distances near a wedge and a cone [15, 16] in binary N₂/N flows. Recent studies [17, 18, 19] also focus on the validation of numerical simulations of nitrogen and air flows near the double cone configuration by the experimental measurements. In [16, 20], comparisons are also made between computed and experimentally determined heat flux and pressure on the cone's surface. In these works, as well as other studies, various models of vibrational-translation relaxation rates and dissociation are used — models which have de-facto become “classical” (see [21, 22, 23, 24, 25, 26]), and more modern models ([27, 28] and others) which are still undergoing approbation. It seems that for cases with a relatively low total enthalpy of the free-stream for simple flow configurations numerical modeling can accurately reproduce experimental data. Description of high-enthalpy non-equilibrium separation flows is a bigger problem [29, 30, 31], and such flows present a large interest as test cases for validation of new and already existing mathematical models of physico-chemical processes.

The objective of this study is to apply the recently developed models of vibration-dissociation coupling to low- and high-enthalpy nonequilibrium separation flows in order to validate them via comparison with experimental data, compare the computation results with those obtained using existing, “classical” models. Another objective is to compare the heat flux computed using different methods, in particular those incorporated into the ANSYS Fluent package and developed in the frame of the kinetic theory of non-equilibrium flows [32, 33, 34]. The kinetic-theory calculations allow one to distinguish contributions of various

processes to the heat transfer and thus help to explain the difference between calculated and measured heat fluxes.

The paper is organised as follows. First we present the computational models with emphasis on vibration-dissociation coupling and transport models. In the next section, we describe the test cases and boundary conditions. Then the simulation results for the double cone and double wedge are discussed as well as possible sources of discrepancy between calculated and measured heat fluxes. Additional aspects such as grid convergence and the role of turbulence are briefly considered in the Appendix.

2. Computational model

In the present work, numerical modeling is done based on the Navier–Stokes equations in the two-temperature approximation, using two different models for vibration-dissociation coupling. It is assumed that the translational and rotational degrees of freedom are in thermal equilibrium, and thus, the translational and rotational temperatures coincide. The vibrational degrees of freedom are in non-equilibrium, meaning that the vibrational temperature of the molecules in the flow is different from the translational temperature and is found solving numerically the conservation equation for the vibrational energy. Numerical solutions of the Navier–Stokes equations were done in the ANSYS Fluent software package augmented by user functions, developed in our previous work [35]. These equations consist of the equations of motion for viscous gases, the energy equation, equations of chemical kinetics with two-temperature reaction rate coefficients, and the vibrational energy relaxation equation. The state equation is the one for the perfect gas with the temperature T corresponding to the local equilibrium degrees of freedom (translational and rotational). The species translational-rotational energy per unit mass is calculated as a function of T with constant specific heats. The vibrational energy per unit mass is calculated as a function of vibrational temperature T_v using the harmonic oscillator model. The detailed description of the mathematical model is given in [35].

The problems are solved in a steady formulation with a density-based solver (specially developed for supersonic and hypersonic flows) with an implicit second-order upwind scheme. The fluxes through the control volume faces are calculated by the AUSM solver [36].

Two flow cases are studied in the work: the flow around a double cone and the flow around a double wedge. The flow around the double cone is a pure molecular nitrogen flow, and dissociation is not taken into account, since the total enthalpy of the free-stream is low. The flow around the double wedge is a high-enthalpy flow of a binary mixture of molecular and atomic nitrogen: N_2/N , and dissociation is accounted for. For the computation of the VT relaxation rate and non-equilibrium dissociation rates, two different models of vibration-dissociation coupling were used; for computation of the equilibrium dissociation rate coefficient, the Arrhenius model parameters were taken according to the recommendations given in [37]. In accordance with [38, 39], it is assumed that during each dissociation event, the total energy of the flow is reduced by the

molecule's dissociation energy, with 70% of the energy being taken from the translation-rotational energy, while the vibrational energy is depleted by 30% of the dissociation energy.

An overview of the models of physico-chemical relaxation and transport processes is presented below.

2.1. Vibration-dissociation model 1

The VT relaxation rate is computed according to the Landau–Teller formula [26]:

$$R^{vibr,VT} = \rho_m \frac{E_{vibr,c}^{eq}(T) - E_{vibr}(T_v)}{\tau^{VT}}. \quad (1)$$

Here ρ_m is the density of molecular nitrogen, T is the translational-rotational temperature of the flow, T_v is the vibrational temperature of the nitrogen molecules, $E_{vibr,c}^{eq}(T)$ is the equilibrium specific vibrational energy, $E_{vibr}(T_v)$ is the specific vibrational energy, and τ^{VT} is the VT relaxation time. VT relaxation time is computed using the Millikan–White formula [40] coupled with Park's high-temperature correction [21].

The Treanor–Marrone model [22] is used to compute dissociation rate coefficients for molecule-molecule and molecule-atom collisions, with the parameter $U = 3T$ providing satisfactory accuracy at high temperatures [41].

2.2. Vibration-dissociation model 2

Within the framework of this model, the VT relaxation rate is computed according to the modified Landau–Teller formula, which is a generalization of the Landau–Teller model for arbitrary deviations from vibrational equilibrium [27, 42]:

$$R^{vibr,VT} = \frac{T}{T_v} (T - T_v) \rho_m \frac{c_v}{\tau^{VT}}. \quad (2)$$

Here c_v is the specific heat of vibrational degrees of freedom. Formula (2) has been obtained from the Boltzmann kinetic equation within the framework of the Chapman–Enskog method by expanding the strict expression for the relaxation term due to VT transitions $R^{vibr,VT(0)}$ into series. It has been shown [27, 8] that this modified Landau–Teller formula gives values of vibrational relaxation rates which are much closer to computations done with strict kinetic theory formula than those given by the original Landau–Teller formula, even under conditions of strong vibrational non-equilibrium.

VT relaxation time is computed via a method developed in [27, 42], as integrals over relative velocity and scattering angles of the vibrational quantum gained/lost during the elementary VT transitions [34]:

$$\frac{1}{\tau^{VT}} = \frac{4kn}{m_m c_v} \left\langle \left(\frac{h\nu}{kT} \right)^2 \right\rangle^{VT}, \quad (3)$$

where n is the number density of the mixture, k is Boltzmann's constant h is Planck's constant, ν is the oscillator frequency, and angular brackets denote

averaging over all possible VT transitions, that is, integration over velocity and scattering angles with corresponding VT transition cross-sections. The Forced Harmonic Oscillator (FHO [43]) model was used for the computation of VT transition cross-sections. For more details on calculation of the VT relaxation times, the reader is referred to [42]. A significant difference between this approach and the Millikan–White formula is that relaxation times computed using definition (3) are functions of both T and T_v . For low temperatures, results given by formula (3) are close to those given by the Millikan–White formula, but at higher temperatures they exhibit non-monotonous behaviour and differ significantly from Millikan–White’s expression.

The Treanor–Marrone model with $U = 3T$ was used to compute dissociation rate coefficients for molecule-molecule collisions. For molecule-atom collisions, a generalized Treanor–Marrone model developed in [37] was used. This generalization of the Treanor–Marrone model is achieved by introducing state-specific parameters U_i for each vibrational level i of the dissociating molecule (instead of a single parameter U). An approximation formula for U_i was obtained by analyzing dissociation rate coefficients computed via quasiclassical trajectory calculations (QCT) and given in [44].

The generalized Treanor–Marrone model gives the following expressions for state-specific dissociation rate coefficients [37]:

$$k_{i,diss}^{N_2} = Z_i(T, U_i) k_{diss,eq}^{N_2}, \quad (4)$$

where $k_{diss,eq}^{N_2}$ is the equilibrium rate coefficient (computed using the Arrhenius law) and $Z_i(T, U_i)$ is the state-specific non-equilibrium factor, defined as

$$Z_i(T, U_i) = \frac{Z_{vibr}(T) \exp\left(-\frac{D}{kU_i}\right)}{\sum_{j=0}^{N_{vib}} \exp\left(-\frac{D - \varepsilon_j}{kU_j}\right)} \exp\left[\frac{\varepsilon_i}{k} \left(\frac{1}{T} + \frac{1}{U_i}\right)\right].$$

where D is the dissociation energy, $Z^{vibr}(T)$ is the equilibrium vibrational partition function, N_{vib} is the number of vibrational levels of N_2 for a harmonic oscillator model, and ε_i is the energy of vibrational level i of the nitrogen molecule. While the general model is suitable for any vibrational ladder, in the present study we use the harmonic oscillator model, $\varepsilon_i = h\nu(i + \frac{1}{2})$.

The approximation for U_i for dissociation reactions for molecule-atom collisions, obtained in [37], has the following form:

$$U_i = \sum_{n=0}^N a_n \tilde{\varepsilon}_i^n \exp\left(T \sum_{k=0}^K b_k \tilde{\varepsilon}_i^k\right),$$

where a_n, b_k are approximation coefficients (see [37]), $\tilde{\varepsilon}_i$ is the vibrational energy of vibrational level i expressed in eV. In order to obtain two-temperature rate coefficients we average the state-specific ones (4) with the non-equilibrium

Boltzmann distribution depending on the vibrational temperature T_v [8].

2.3. Models of transport processes

While solving the Navier–Stokes equations in the ANSYS Fluent software package, the following model of transport processes is used. The dynamic viscosity and thermal conductivity coefficients of the gas mixture are calculated by Wilke's mixing rule [45]. The viscosity, thermal conductivity, and binary diffusion coefficients for individual components of the gas mixture are calculated on the basis of the Hirschfelder model [46]. These dependencies correspond to the “ideal-gas-mixing-law” option for the viscosity and thermal conductivity coefficients of the entire mixture (the “kinetic-theory” option was used for individual components of the mixture), and the “kinetic theory” option was used for calculating the effective diffusion coefficient.

In order to assess the basic tools incorporated to ANSYS Fluent, more rigorous transport algorithms developed in [32, 33, 34] for strongly non-equilibrium reacting flows have been also applied. In these studies, the expressions for the diffusive and heat fluxes are derived within the framework of the generalized Chapman-Enskog method. In the general case, the heat flux in the two-temperature flows takes the form:

$$\mathbf{q} = \mathbf{q}_{t-r} + \mathbf{q}_v + \mathbf{q}_{MD} + \mathbf{q}_{TD}, \quad (5)$$

where \mathbf{q}_{t-r} , \mathbf{q}_v , \mathbf{q}_{MD} , \mathbf{q}_{TD} are the energy fluxes associated with the thermal conductivity of translational and rotational degrees of freedom, thermal conductivity of vibrational degrees of freedom, mass diffusion and thermal diffusion, correspondingly.

For binary mixtures, we have the following expressions of these contributions to the total heat flux:

$$\begin{aligned} \mathbf{q}_{t-r} &= \lambda' \nabla T, \\ \mathbf{q}_v &= \lambda_v \nabla T_v, \\ \mathbf{q}_{MD} &= \rho_m h_m (-D_{mm} \mathbf{d}_m - D_{ma} \mathbf{d}_a) + \rho_a h_a (-D_{ma} \mathbf{d}_m - D_{aa} \mathbf{d}_a), \\ \mathbf{q}_{TD} &= -p (D_{Tm} \mathbf{d}_m + D_{Ta} \mathbf{d}_a) - \rho_m h_m D_{Tm} \nabla \ln T - \rho_a h_a D_{Ta} \nabla \ln T, \end{aligned} \quad (6)$$

where λ' is the partial thermal conductivity of translational and rotational degrees of freedom, λ_v is the thermal conductivity of vibrational degrees of freedom, D_{Tm} , D_{Ta} , D_{mm} , D_{ma} , D_{aa} are the thermal diffusion and multicomponent diffusion coefficients, h_m , h_a are the specific enthalpies of molecular and atomic components, \mathbf{d}_c is the diffusive driving force for the species c depending on the gradients of species molar fraction and pressure.

The transport coefficients are found using the kinetic theory algorithm in the two-temperature approximation [34]. This method gives the transport coefficients as solutions of linear transport systems. The systems contain bracket integrals as coefficients, which could be expressed via collision $\Omega^{(l,r)}$ -integrals depending on the molecular interaction potential. The most reliable available data on the collision integrals [47] are used in our simulations.

To calculate the heat flux given by the kinetic-theory algorithm, the post-processing procedure is applied in the present study. Having the flow variables from our simulations, we substitute them to the linear systems for the calculation of transport coefficients expressions. Then the transport coefficients and derivatives of flow variables are substituted to the expressions for the different terms in the heat flux, and the total heat flux is computed.

It is worth noting that the contribution of thermal diffusion, \mathbf{q}_{TD} , is systematically neglected in the computational fluid dynamics due to the common assumption of its weak influence on the flow. Thus in the simulations performed in this work, thermal diffusion is not taken into account. However in the kinetic-theory simulations we include thermal diffusion while calculating the heat flux. In the next section we compare the results obtained using both techniques and evaluate the role of various dissipative processes in the heat transfer.

3. Problem formulation and boundary conditions

We consider a flow of molecular nitrogen around a double cone and a binary nitrogen flow (N_2/N) around a double wedge. These flows were studied experimentally in [48, 49, 29]. Free-stream conditions are given in Table 1 for the double cone flow case and in Table 2 for the flow around a double wedge. The flow around the double cone was considered for an attack angle equal to 0; for the double wedge flow we considered three cases with different values of the attack angle α . In the double wedge case, the mass fraction of atomic nitrogen in the free-stream was taken to be equal to $Y_{N,\infty}$. The conditions for the flow around a double cone are taken from [50] (see also Ref. 6 in the latter paper), and for the flow around a double wedge from [29].

Table 1: Free-stream conditions for the double cone case

$T_{tr,\infty}$, K	$T_{v,\infty}$, K	p_∞ , Pa	v_∞ , m/s	h_0 , MJ/kg
42.6	1986	2.23	2073	2.1

Table 2: Free-stream conditions for the double wedge test cases

Run	v_∞ , m/s	T_∞ , K	$T_{v,\infty}$	ρ_∞ , kg/m ³	$Y_{N,\infty}$	α , deg	h_0 , MJ/kg
1049	6110	1888	3856	0.0078	0.129	0	26.1
1043	6059	1841	3851	0.0076	0.125	12.0	25.7
1038	6068	1710	3758	0.0065	0.128	10.0	27.3

Solution domains used in the present work are shown on fig. 1a for the double cone case and fig. 1b for the double wedge case. Free-stream conditions were set on the left boundary (inlet); for the right boundary (outlet) conditions,

all variables were extrapolated out of the computational domain. The cone and wedge walls were considered to be isothermic at a temperature of $T_w = 300$ K, and no-slip conditions for the walls were used, along with the following constraints on the surface gradients: a zero gradient of pressure, a zero gradient of diffusive flux (for the double wedge case). The last condition corresponds to the non-catalytic surface which is justified by low activity of nitrogen on metallic surfaces. Moreover the surface is assumed isothermal for the vibrational mode, and the vibrational energy on the surface is calculated using the Boltzmann distribution with the wall temperature.

The flow around the double cone was considered to be axisymmetric, therefore a condition of axial symmetry was set on the lower boundary (axis). The flow around the double wedge was considered to be planar, therefore a symmetry condition on the lower boundary was set for Run 1049 (test case with an attack angle $\alpha = 0$); for all other cases of the double wedge flow, extrapolation of all variables out of the computational domain was used.

Computations were performed on a structured quadrilateral mesh, refined near the surface of the body. After a numerical solution had been obtained, the mesh was refined by splitting each cell in two in each direction from the shock wave to the body. This procedure was repeated until convergence of the numerical solutions was achieved.

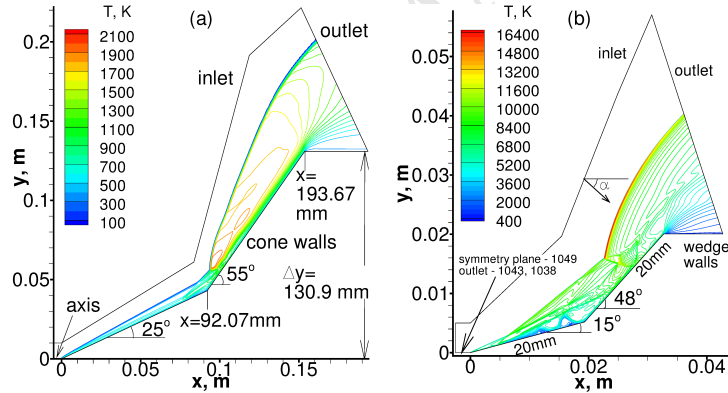


Figure 1: Computational domains for double cone (a) and double wedge (b). Contours show translational-rotational temperature, obtained in computations with vibration-dissociation model 2. Case 1038 for double wedge is shown.

For the considered flow configurations, an attached shock appears at the frontal part of the body, which interacts with a detached shock wave (the latter is detached from the second part of the cone or wedge). Due to this interaction, a shock wave configuration similar to that described in [51] appears. In such flow configurations a separation zone with one or more vortices appears on the surface near the inflection point. Depending on the free-stream flow parameters, interference of the shock waves leads to development of shear layers emanating from the region of shock wave interaction.

4. Results

In this section, results of numerical modeling of flows around a double cone and double wedge are compared with available experimental data [48, 49, 29].

4.1. Double cone

Flowfields for the flow around a double cone are shown in fig. 2. For modeling VT relaxation model 2 was used. An area of maximum pressures appears behind the detached shock wave from the second part of the double cone (fig. 2a,b) due to interference between it and the shock wave, emanating from the cone apex. For the flowfield in the separation zone (fig. 2b), streamlines visualizing one vortex are shown with arrows. Continuous lines level 0-2 denote the boundaries of the grid adaption; it can be seen that the whole shock wave structure is located inside the zone of grid cell refinement. Translational-rotational and vibrational temperatures are shown on fig. 2c,d, correspondingly. Nitrogen molecules begin to dissociate at temperatures $T \geq 4000$ K; since temperatures in the considered flow case do not exceed 2100 K, dissociation of N₂ can be neglected.

A comparison of experimental data [48, 49] on pressure and heat flux on the double cone surface and results of numerical modeling using various VT relaxation models is shown in fig. 3. Results of numerical modeling using different vibrational relaxation models give good agreement with each other and experimental results. To assess the influence of vibrational excitation, a computation has been performed in which the vibrational degrees of freedom are fully frozen (curve “no vibrations”). It can be seen that the vibrational relaxation has no influence on the pressure distribution on the cone surface (fig. 3a). On fig. 3b we can see a good agreement of results of modeling with vibrational non-equilibrium with experimental data on the distribution of the heat flux (to be consistent with the experimental results, we give the absolute value of the heat flux although under conditions of cold wall the heat flux is negative). When the vibrational degrees of freedom are assumed to be frozen, the heat flux is underestimated, however the discrepancy does not exceed 9% which is within the range of experimental uncertainty. Because of slow relaxation of the gas behind the detached shock wave (due to low translation-rotational temperature in that region) the vibrational degrees of freedom are practically frozen. Based on this, we can conclude that vibrational non-equilibrium has an insignificant effect on the flow parameters on the double cone surface for the considered set of free-stream and boundary conditions.

4.2. Double wedge

Heat fluxes on the double wedge surface computed using various models are shown on fig. 4 for three different test cases. Figure 4 also shows experimental data [29] and numerical modeling results [30]. It can be seen that all numerical simulations give a qualitative agreement with experimental measurements, but underestimate the heat flux. Differences in the numerical modeling results can be connected with using different vibration-dissociation coupling models as well as different models for the transport coefficients. We see the existence of multiple

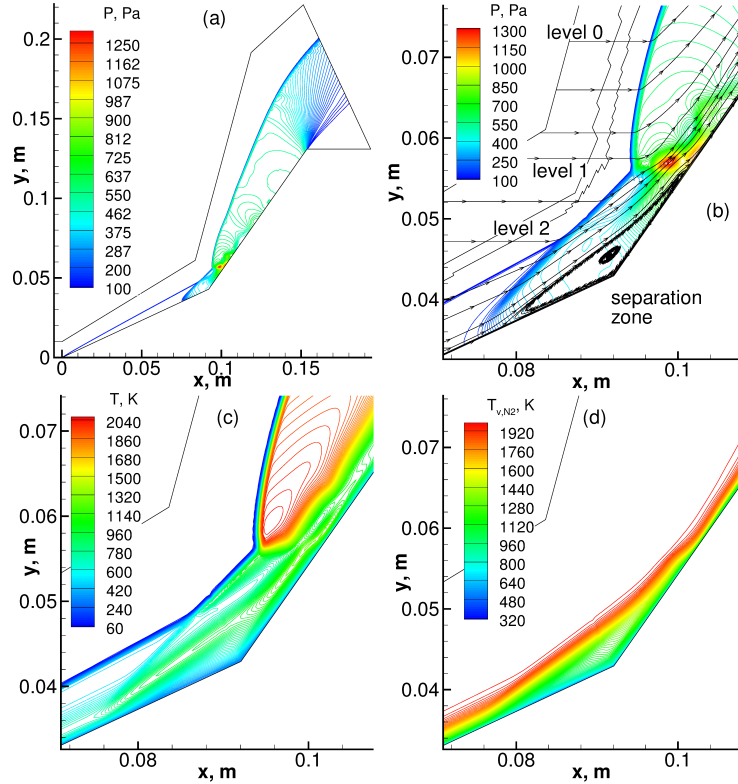


Figure 2: Pressure contours in the whole computational domain (a) and in the separation region (b), translational-rotational temperature (c) and vibrational temperature (d). Computations were performed using model 2.

local minima and maxima of the heat flux, caused by the vortex structure in the separation zone.

A comparison of flowfields in the separation region for the case 1038, computed using various models, is shown on figs. 5 and 6. Different columns correspond to different vibration-dissociation coupling models, while different rows correspond to different flow parameters. We see that use of different vibration-dissociation models leads to a significant change in the shock detachment point on the first wedge and a change in the shock stand-off distance for the second wedge. We see from figs. 5a,b that the region of maximum pressure changes in size. The vortex structure in the separation zone also changes significantly, which is seen from figs. 5c,d, where arrows denote the streamlines. Use of different models of vibration-dissociation coupling also leads to a marked change in the mixture composition, which can be seen from the distribution of the mass fraction of atomic nitrogen as shown on fig. 5c,d.

Values of translational-rotational and vibrational temperatures obtained using different models are shown on fig. 6. Both the translational-rotational and vi-

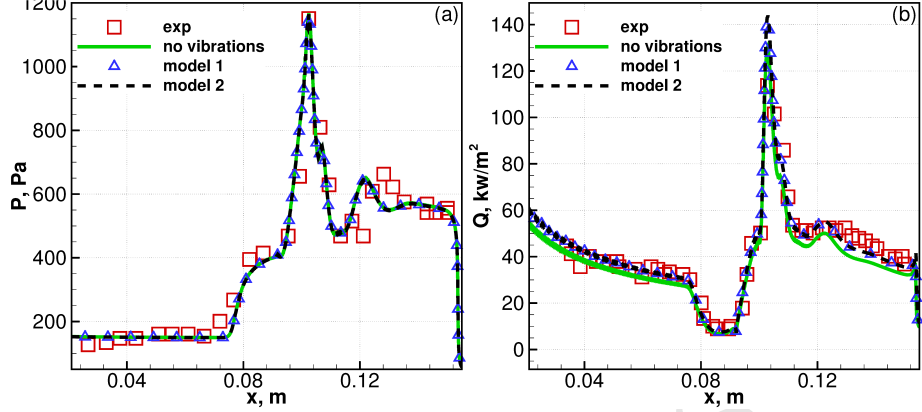


Figure 3: Pressure (a) and heat flux (b) on double cone surface.

brational temperatures reach their maximum values behind the detached shock waves, and on fig. 6c,d we see a narrow excitation zone, in which the vibrational temperature of nitrogen molecules rises due to TV transitions, i.e. the transition of translational-rotational energy to the vibrational mode, which leads to: 1) a decrease of the translational-rotational temperatures as the distance from the shock front increases 2) an increase in the dissociation rate.

For more detailed analysis of the numerical results obtained using the two models of VT relaxation, a comparison was performed of the mass fraction of atomic nitrogen and the gas temperature along lines perpendicular to the wedge surface. This comparison is shown on fig. 7. Distributions of the flow parameters along lines L1-L4 are shown as functions of x , where the gas flows in the direction of increasing x . Near the leading edge of the double wedge the mass fraction of atomic nitrogen is significantly larger when model 2 is used, but further downstream both models give close results. The temperature distributions show that use of model 2 leads to a noticeably faster equilibration of translational-rotational and vibrational degrees of freedom, which affects the dissociation rate.

In order to understand possible sources of discrepancy in the calculated and measured heat fluxes we evaluated different contributions to the total heat flux along the lines L1-L3 using both rigorous methods of kinetic theory and basic tools incorporated into the flow-solver. In Table 3, different terms in the surface heat flux are compared. In order to be consistent with the above discussion, we give absolute values of q_{t-r} , and q_v which are indeed negative on the surface. Note that in the left two columns, q_{t-r} is calculated directly by the CFD-solver whereas q_v is computed by the user defined function; thermal diffusion in these simulations is neglected according to the common practice in the computational fluid dynamics. Mass diffusion flux q_{MD} on the surface is zero since the surface is non-catalytic. One can see that both methods give

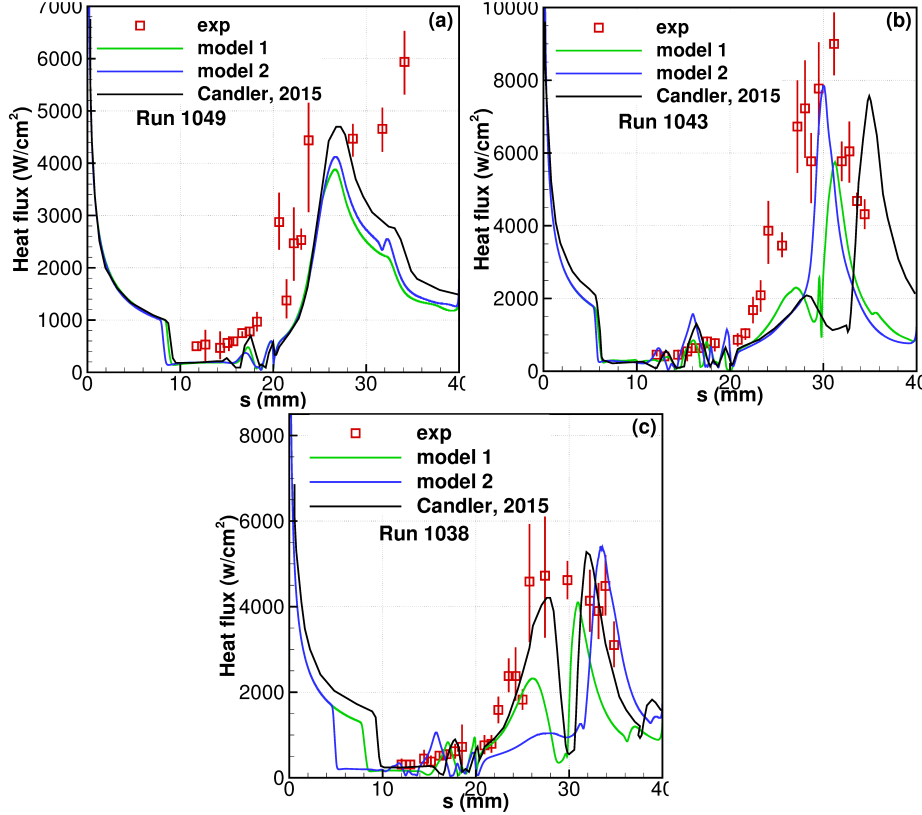


Figure 4: Heat flux on double wedge surface.

rather close values of translational–rotational energy flux q_{t-r} (the difference does not exceed 5–6%). On the other hand, the chosen flow solver systematically underestimates the vibrational energy flux q_v , the discrepancy is about 20–30%. The heat flux due to thermal diffusion q_{TD} may play a crucial role in the heat transfer near non-catalytic surfaces. Whereas it is neglected in CFD simulations, in the kinetic-theory calculations it is comparable to q_{t-r} but has an opposite sign; this leads to a significant decrease in the total energy flux q at the surface. A similar effect is discussed in [52, 53]. For partially catalytic surfaces, the effect of mass diffusion in the heat transfer becomes dominant, and the contribution of thermal diffusion is much weaker. Therefore one of the reasons for the discrepancy between measured and calculated heat flux can be neglecting the catalytic activity on the surface (if the surface material used in the experiments is not fully non-catalytic). Other potential reasons can be omission of thermal diffusion effects (if the surface is indeed fully non-catalytic) and possibility of three-dimensional effects in the experiment as discussed in Section 5. These issues require further study.

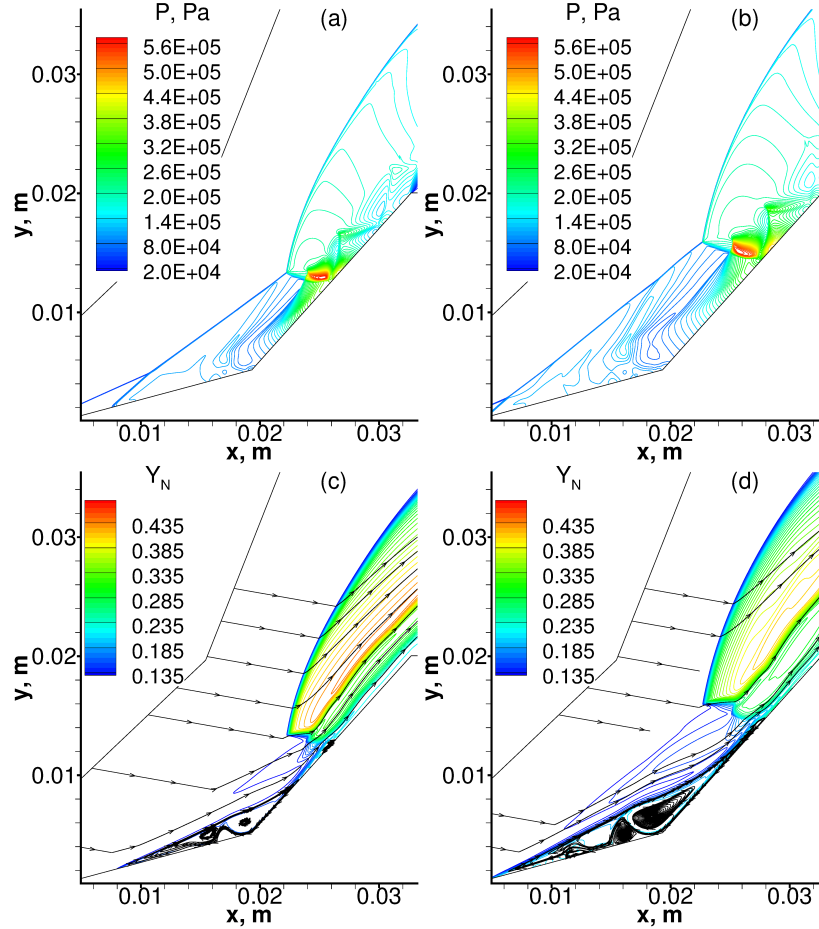


Figure 5: Comparison of pressure (a,b) and mass fraction of atomic nitrogen (c,d) obtained in computations with models 1 (a,c) and 2 (b,d). Case 1038.

Now let us consider the heat flux calculated in the direction normal to the surface. While the contribution of thermal diffusion to the total heat flux is important at the surface, it is small (less than 5%) at some distance from the wall. Therefore we do not include q_{TD} in the further discussion. On fig. 8, the energy fluxes due to thermal conductivity of translational–rotational degrees of freedom (\mathbf{q}_{t-r}) and due to the thermal conductivity of vibrational degrees of freedom (\mathbf{q}_v) are presented. Results for computations performed with the 1st model of vibration-dissociation coupling are shown with solid lines, results for computations performed with the 2nd model – with dashed lines. Since the contribution of these fluxes to the total heat flux are proportional to the gradients of the translational-rotational and vibrational temperatures, correspondingly, the contribution of \mathbf{q}_{t-r} is significantly larger than \mathbf{q}_v . We see that the fluxes

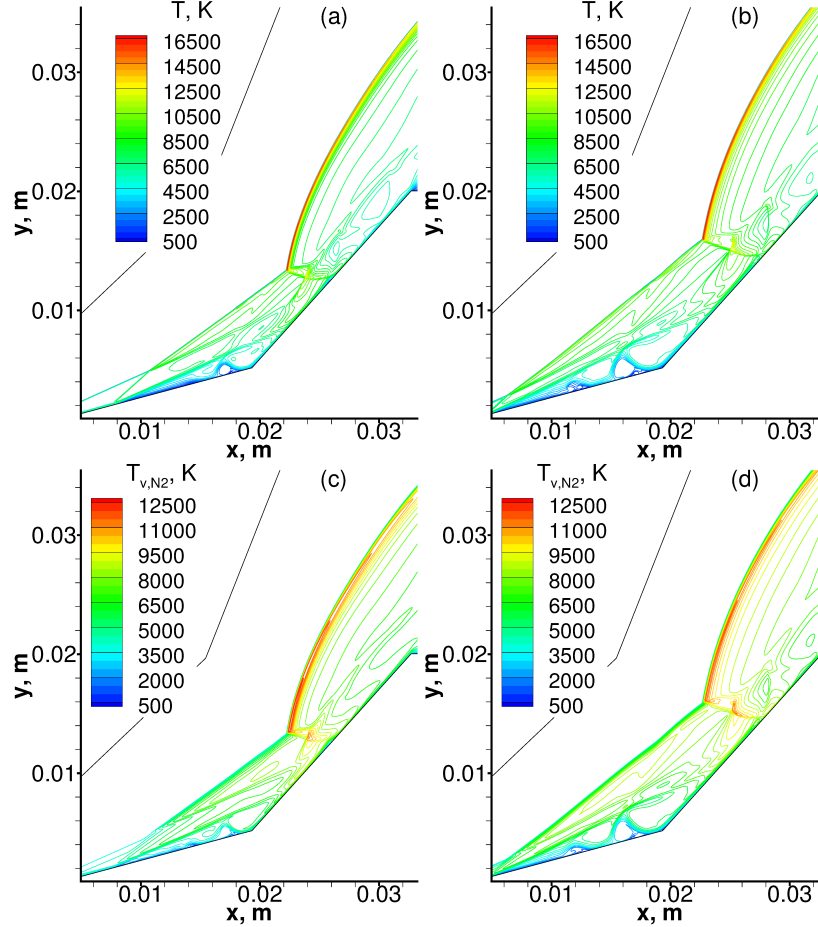


Figure 6: Comparison of translational-rotational (a,b) and vibrational (c,d) temperatures obtained in computations with models 1 (a,c) and 2 (b,d). Case 1038.

change the sign along the normal; for model 1 the peak of the heat flux is closer to the double wedge's surface,

Next, we compare the heat fluxes due to the thermal conductivity of translational-rotational degrees of freedom (\mathbf{q}_{t-r}) and due to the mass diffusion (\mathbf{q}_{MD}) (fig. 9). We see that the contribution of these fluxes to the total heat flux are commensurable almost along the entire length of the lines normal to the double wedge, except the region near the body surface where \mathbf{q}_{t-r} is substantially higher than \mathbf{q}_{MD} since the surface is non-catalytic, and \mathbf{q}_{MD} is close to zero. These fluxes are the largest contributors to the total heat flux; the peaks of the \mathbf{q}_{t-r} and \mathbf{q}_{MD} fluxes are comparable both in intensity and location.

For the total heat flux on lines L1, L3 (fig. 10) we get the same general picture that has been obtained for the flowfield in general. Multiple maxima and

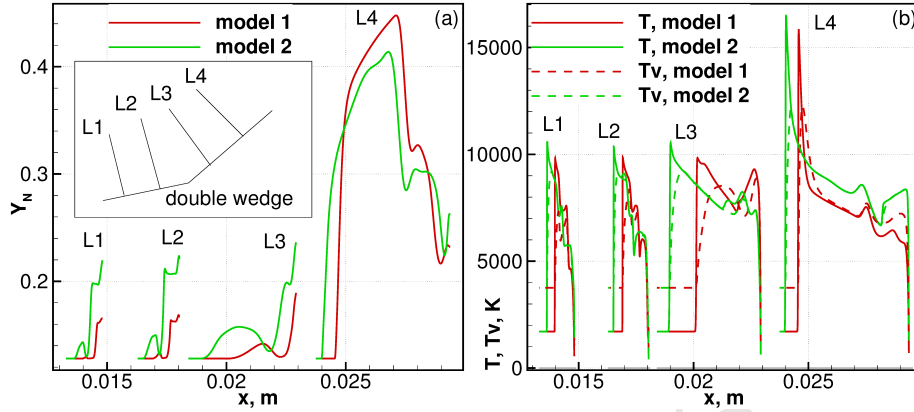


Figure 7: Comparison of atomic nitrogen mass fraction (a) and translational-rotational and vibrational temperatures (b) along the lines normal to the double wedge surface. Case 1038.

Table 3: Comparison of the energy fluxes calculated using the algorithm implemented in ANSYS Fluent and kinetic theory algorithms (KT), q , kW/cm^2 .

Case	q_{t-r}	q_v	q_{t-r}	q_v	q_{TD}
	ANSYS Fluent		KT		
Model 1, L1	118.98	12.31	120.63	15.09	-119.53
Model 1, L2	134.6	23.5	135.63	30.58	-124.15
Model 1, L3	1912.39	310.35	1794.19	469.89	-463.29
Model 2, L1	747.74	85.69	722.24	120.84	-399.58
Model 2, L2	128.5	6.32	130.09	7.13	-143.54
Model 2, L3	786.82	72.95	753.64	101.68	-383.9

minima of the heat flux exist due to the vortex structure in the flow separation zone.

5. Discussion

Surface-distributed characteristics (pressure and heat flux) can be accurately predicted on a double cone surface in a hypersonic flow without chemical reactions, using Navier–Stokes equations in a two-temperature approximation. In this case VT relaxation has practically no effect on the pressure, heat flux and the flowfield. Good agreement with experimental data is due to absence of three-dimensional effects (the body is axisymmetric) and chemical reactions, along with practically frozen vibrational degrees of freedom. In this case only one vortex appears in the separation zone, which significantly simplifies prediction of the surface characteristics.

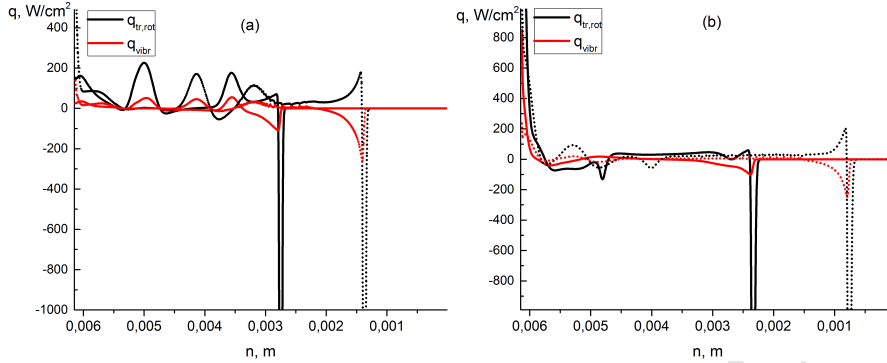


Figure 8: Comparison of the energy fluxes associated with the thermal conductivity of translational and rotational degrees of freedom and thermal conductivity of vibrational degrees of freedom along the lines normal to the double wedge surface. (a) – L1, (b) – L3. Model 1 – solid lines, model 2 – dash lines.

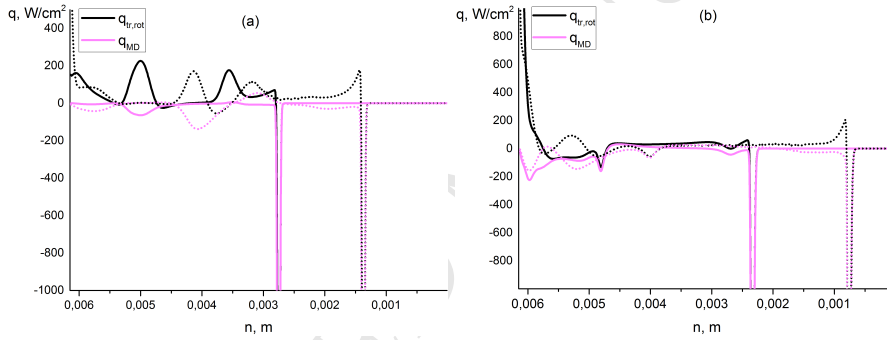


Figure 9: Comparison of the energy fluxes associated with the thermal conductivity of translational and rotational degrees of freedom and mass diffusion along the lines normal to the double wedge surface. (a) – L1, (b) – L3. Model 1 – solid lines, model 2 – dashed lines.

Heat fluxes computed on the double wedge surface in a high-enthalpy dissociating flow of N_2/N qualitatively agree with experimental data [29]. Similar behaviour is observed for numerical results of other authors [30]. There is a variety of potential reasons for the quantitative discrepancy of simulation results and experimental data, among them the choice of model for vibration-dissociation coupling, the model for the calculation of transport properties, neglecting thermal diffusion and catalytic activity on the wall, presence of three-dimensional effects, possible laminar-turbulent transition.

Calculations show that the vibration-dissociation coupling model can significantly affect the shock waves configuration, the separation zone and the structure of vortices in it, shock detachment, and mixture composition (fig. 5 and fig. 6). Use of different recommended values for the computation of the equilibrium dissociation rate coefficient can also lead to differing results, which has been noted in [29]. Significant changes in the flow structure lead to a change

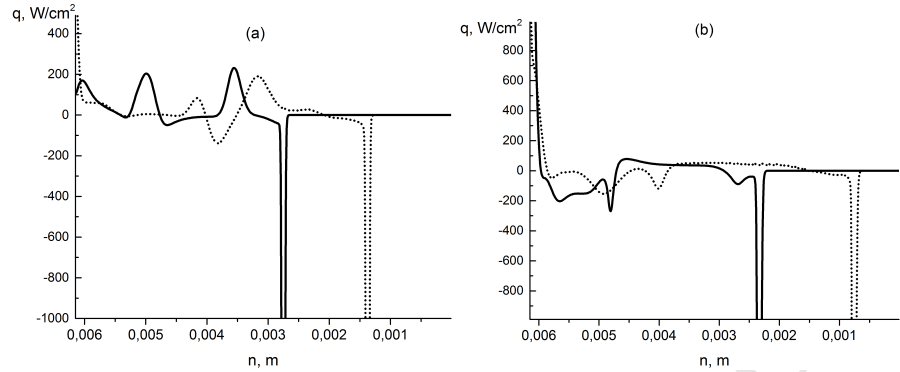


Figure 10: Total heat flux along the lines normal to the double wedge surface. (a) – L1, (b) – L3. Model 1 – solid lines, model 2 – dashed lines.

in the heat flux distribution on the wedge surface.

In the present work we considered a planar flow, assuming negligibility of three-dimensional effects. They can have an influence on the inclination of the shock wave, causing a change in the Mach number in the direction perpendicular to the discontinuity surface, and, correspondingly, causing a change in the shock intensity. An example of the influence of three-dimensional flow effects is the so-called hybrid shock reflection [54] in a stationary flow between two symmetrically located wedges. Hybrid reflection occurs only in the three-dimensional case – regular reflections are formed on the edges, and in the central plane Mach reflection occurs, the structure of which differs significantly from the Mach reflection's structure in a planar flow. The structure and intensity of the shocks in the considered double wedge case might also depend on three-dimensional effects. To the authors knowledge, three-dimensional effects have not been studied for a high-enthalpy flow around a double wedge.

The flow around a double wedge includes several shear layers, vortices in the flow separation region, and multiple shock wave intersections. Due to the instability of the shear layers, perturbations are formed, which affect the flow structure. In this case, local laminar-turbulent transitions are possible, and since in turbulent flows heat fluxes on a body's surface are usually higher than in laminar flows, this can possibly explain the underestimation of the heat flux (in comparison with experimental data) in several regions as shown on fig. 4. After a region of turbulent flow, a reverse transition to a laminar flow should follow, since the Reynolds number, based on the free-stream parameters and length of the double wedge, is quite low $Re \sim 3 \cdot 10^4$ (for example, in [55] was shown that for a cold gas the lowest transition boundary on the cone is approximately $Re_{tr} \sim 1.5 \cdot 10^6$). The hypothesis of the transition from laminar to turbulent flow and back requires an accurate test. For this purpose numerical modeling using high-order schemes with low dissipation should probably be performed, analogous to the testing done in [56] for modeling of the laminar-turbulent transition on a flat plate. The possible role of laminar-turbulent transitions is

assessed in AppendixB.

An additional factor affecting the heat flux on the double wedge surface can be the use of overly simplified boundary conditions, more specifically, the no-slip condition. At low Reynolds numbers rarefaction effects may be important; within the framework of the Navier–Stokes equations they can be accounted for via boundary conditions of slip and temperature jump. In [57] it has been shown with numerical modeling that for a free-stream Mach number $M_\infty \sim 10$ and Reynolds number $Re_\infty \sim 2 \cdot 10^4$ in a gas flow with low enthalpy a more accurate boundary condition has some effect on the numerical solution.

It can be concluded that a high-enthalpy non-equilibrium flow around a double wedge with flow separation is a good test for validation of mathematical models for gas flow description. At the same time, a detailed study of the aforementioned effects on the distribution of the heat flux remains a question for further investigation.

6. Conclusions

Numerical modeling based on two-temperature Navier–Stokes equations allows for an accurate prediction of heat fluxes and pressure distribution on a double cone surface in a high-velocity stream of molecular nitrogen with a low total enthalpy. Despite a good agreement with experimental data, this test case does not allow for validation of mathematical models of VT relaxation, since it practically does not affect the surface characteristics.

Computations of a high-enthalpy non-equilibrium binary nitrogen N₂/N flow with separation around a double wedge qualitatively reproduce experimental measurements of heat flux on its surface. For this test case, VT relaxation and dissociation reactions have a strong influence on the distribution of the heat flux on the double cone surface. Despite the quantitative differences between the numerical and experimental data, the double wedge flow can be considered a test for validation of models of vibration-dissociation coupling. However, for more accurate validation of these models a further study of the processes affecting the heat flux distribution is needed.

7. Acknowledgments

This work was supported by the Russian Science Foundation (Grant No. 15-19-30016). Computational resources were kindly provided by Siberian Supercomputer Center of the Institute of Computational Mathematics and Mathematical Geophysics (sscc.ru), Computational Center of Novosibirsk State University (nusc.nsu.ru) and Supercomputer center of Saint Petersburg State University.

8. References

- [1] H. Weihs, J. Longo, J. Turner, The sharp edge flight experiment SHEFEX II, a mission overview and status, 15th AIAA International Space

Planes and Hypersonic Systems and Technologies Conference, 2008. AIAA Paper 2008-2542.

- [2] Y. Li, B. Reimann, T. Eggers, Coupled simulation of CFD-flight-mechanics with a two-species-gas-model for the hot rocket staging, *Acta Astronautica* 128 (2016) 44 – 61.
- [3] T. Gawehn, D. Neeb, F. Tarfeld, A. Güilhan, M. Dormieux, P. Binetti, T. Walloschek, Experimental investigation of the influence of the flow structure on the aerodynamic coefficients of the IXV vehicle, *Shock Waves* 21 (3) (2011) 253–266.
- [4] L. Ibraguimova, A. Sergievskaya, V. Levashov, O. Shatalov, Y. Tunik, I. Zabelinskii, Investigation of oxygen dissociation and vibrational relaxation at temperatures 4000-10800 K, *Journal of Chemical Physics* 139 (2013) 034317.
- [5] I. Wysong, S. Gimelshein, Y. Bondar, M. Ivanov, Comparison of direct simulation Monte Carlo chemistry and vibrational models applied to oxygen shock measurements, *Phys. Fluids* 26 (2014) 043101.
- [6] K. Neitzel, D. Andrienko, I. Boyd, Aerothermochemical nonequilibrium modeling for oxygen flows, *Journal of Thermophysics and Heat Transfer* 31 (3) (2017) 634–645.
- [7] V.Yu. Gidashev, S.A. Losev, N.S. Severina, Nonequilibrium kinetics in oxygen dissociation behind a shock wave front, *Mathematical Models and Computer Simulations* 2 (2) (2010) 211–221.
- [8] E. Kustova, E. Nagnibeda, G. Oblapenko, A. Savelev, I. Sharafutdinov, Advanced models for vibrational-chemical coupling in multi-temperature flows, *Chem. Phys.* 464 (2016) 1–13.
- [9] G. Candler, R. MacCormack, Computation of weakly ionized hypersonic flows in thermochemical nonequilibrium, *J. Thermophysics and Heat Transfer* 5 (3) (1990) 266–273.
- [10] A. Shevyrin, Y. Bondar, S. Kalashnikov, V. Khlybov, V. Degtyar', Direct simulation of rarefied high-enthalpy flow around the RAM C-II capsule, *High Temperature* 54 (3) (2016) 383–389.
- [11] S. Surzhikov, Two-dimensional numerical analysis of flow ionization in the RAM-C-II flight experiment, *Russian Journal of Physical Chemistry B* 9 (1) (2015) 69–86.
- [12] J. Hao, J. Wang, C. Lee, Numerical study of hypersonic flows over reentry configurations with different chemical nonequilibrium models, *Acta Astronautica* 126 (2016) 1–10.

- [13] Y. Bondar, G. Markelov, S. Gimelshein, M. Ivanov, Numerical modeling of near-continuum flow over a wedge with real gas effects, *Journal of Thermophysics and Heat Transfer* 20 (4) (2006) 699–709.
- [14] H. G. Hornung, G. H. Smith, The influence of relaxation on shock detachment, *Journal of Fluid Mechanics* 93 (2) (1979) 225–239.
- [15] N. Petrov, S. Kirilovskiy, T. Poplavskaya, G. Shoev, A numerical study of non-equilibrium flows with different vibrational relaxation models, *Technical Physics Letters* 42 (7) (2016) 697–700.
- [16] I. A. Leyva, Shock detachment processes on cones in hypervelocity flows, Ph.D. thesis, California Institute of Technology (1999).
- [17] D. Knight, J. Longo, D. Drikakis, D. Gaitonde, A. Lani, I. Nompelis, B. Reimann, L. Walpot, Assessment of cfd capability for prediction of hypersonic shock interactions, *Progress in Aerospace Sciences* 48 (2012) 8–26.
- [18] M. Rouhi Youssefi, D. Knight, Assessment of CFD capability for high enthalpy non-equilibrium flows with strong viscous-inviscid interaction, 53rd AIAA Aerospace Sciences Meeting, 2015, AIAA Paper 2015-0580.
- [19] J. Hao, J. Wang, C. Lee, Numerical simulation of high-enthalpy double-cone flows, *AIAA Journal* 55 (7) (2017) 2471–2475.
- [20] O. Kunova, E. Kustova, M. Mekhonoshina, G. Shoev, Numerical simulation of coupled state-to-state kinetics and heat transfer in viscous non-equilibrium flows, *AIP Conference Proceedings* 1786 (2016) 070012.
- [21] C. Park, *Nonequilibrium Hypersonic Aerothermodynamics*, John Wiley and Sons, New York, NY, 1990.
- [22] P. Marrone, C. Treanor, Chemical relaxation with preferential dissociation from excited vibrational levels, *Physics of Fluids* 6 (9) (1963) 1215–1221.
- [23] S. Macheret, A. Fridman, I. Adamovich, J. Rich, C. Treanor, 6th AIAA/ASME Joint Thermophysics and Heat Transfer Conference, June 20-23, 1994, Colorado Springs, CO (AIAA Paper 94-1984).
- [24] S.A. Losev, N.A. Generalov, To the investigation of oscillations excitation and oxygen molecules decay under high temperatures, *Dokl. Akad. Nauk USSR* 5 (141) (1961) 1072–1077.
- [25] N. Kuznetsov, *Kinetics of Monomolecular Reactions*, Moscow: Nauka, 1982.
- [26] L. Landau, E. Teller, *Collected Papers*, Vol. 1, Moscow: Nauka, 1969.

- [27] E. Kustova, G. Oblapenko, Reaction and internal energy relaxation rates in viscous thermochemically non-equilibrium gas flows, *Phys. Fluids* 27 (2015) 016102.
- [28] Y. Gorbachev, Gas-dynamic equations for spatially inhomogeneous gas mixtures with internal degrees of freedom. III. renormalized reaction rates, *Applied Mathematical Modelling* 40 (23–24) (2016) 10131–10152.
- [29] J. Olejniczak, G. Candler, M. Wright, I. Leyva, H. Hornung, Experimental and computational study of high enthalpy double-wedge flows, *Journal of Thermophysics and Heat Transfer* 13 (4) (1999) 431–440.
- [30] G. Candler, Rate-dependent energetic processes in hypersonic flows, *Progress in Aerospace Sciences* 72 (2015) 37–48, celebrating 60 Years of the Air Force Office of Scientific Research (AFOSR): A Review of Hypersonic Aerothermodynamics.
- [31] R. Prakash, S. Gai, S. O’Byrne, M. Brown, Dsmc computations of hypersonic flow separation and re-attachment in the transition to continuum regime, *AIP Conference Proceedings* 1786 (2016) 050012.
- [32] A. Chikhaoui, J. Dudon, E. Kustova, E. Nagnibeda, Transport properties in reacting mixture of polyatomic gases, *Physica A* 247 (1-4) (1997) 526–552.
- [33] A. Chikhaoui, J. Dudon, S. Genieys, E. Kustova, E. Nagnibeda, Multi-temperature kinetic model for heat transfer in reacting gas mixture, *Physics of Fluids* 12 (1) (2000) 220–232.
- [34] E. Nagnibeda, E. Kustova, *Nonequilibrium Reacting Gas Flows. Kinetic Theory of Transport and Relaxation Processes*, Springer, Berlin, 2009.
- [35] G. Shovev, Y. Bondar, G. P. Oblapenko, E. Kustova, Development and testing of a numerical simulation method for thermally nonequilibrium dissociating flows in ANSYS Fluent, *Thermophysics and Aeromechanics* 23 (2) (2016) 151–163.
- [36] M. S. Liou, C. J. Steffen, Jr., A new flux splitting scheme, *Journal of Computational Physics* 107 (1) (1993) 23–39.
- [37] O. Kunova, E. Kustova, A. Savelev, Generalized Treanor–Marrone model for state-specific dissociation rate coefficients, *Chem. Phys. Lett.* 659 (2016) 80–87.
- [38] P. Gnoffo, R. Gupta, J. Shinn, Conservation equations and physical models for hypersonic air flow in thermal and chemical non-equilibrium, *NASA Technical Paper NASA-TP-2867* (1989) 1–61.
- [39] S. Sharma, W. Huo, C. Park, Rate parameters for coupled vibration-dissociation in a generalized SSH approximation, *Journal of thermophysics and heat transfer* 6 (1) (1992) 9–21.

- [40] R. Millikan, D. White, Systematics of vibrational relaxation, *Journal of Chemical Physics* 39 (12) (1963) 3209–3213.
- [41] F. Esposito, M. Capitelli, E. Kustova, E. Nagnibeda, Rate coefficients for the reaction $N_2(i)+N=3N$: a comparison of trajectory calculations and the Treanor-Marrone model., *Chem. Phys. Lett.* 330 (2000) 207–211.
- [42] E. Kustova, G. Oblapenko, Mutual effect of vibrational relaxation and chemical reactions in viscous multitemperature flows, *Phys. Rev. E* 93 (2016) 033127.
- [43] I. Adamovich, S. Macheret, J. Rich, C. Treanor, Vibrational energy transfer rates using a forced harmonic oscillator model, *Journal of Thermophysics and Heat Transfer* 12 (1) (1998) 57–65.
- [44] Planetary entry integrated models, <http://phys4entrydb.ba.imip.cnr.it/Phys4EntryDB/>.
- [45] C. R. Wilke, A viscosity equation for gas mixtures, *J. Chem. Phys.* 18 (1950) 517–519.
- [46] J. O. Hirschfelder, C. F. Curtiss, R. B. Bird, *Molecular theory of gases and liquids*, Wiley New York, 1954.
- [47] D. Bruno, M. Capitelli, C. Catalfamo, R. Celiberto, G. Colonna, P. Diomede, D. Giordano, C. Gorse, A. Laricchiuta, S. Longo, D. Pagano, F. Pirani, Transport properties of high-temperature mars-atmosphere components, *ESA STR 256*, ESA, Noordwijk: ESA Publications Division (2008).
- [48] M. Holden, Experimental studies of laminar separated flows induced by shock wave/boundary layer and shock/shock interaction in hypersonic flows for CFD validation, January 2000, AIAA Paper 2000-0930.
- [49] M. Holden, T. Wadhams, Code validation study of laminar shock/boundary layer and shock/shock interactions in hypersonic flow, part A: Experimental measurements, 39th Aerospace Sciences Meeting and Exhibit, Reno, NV, January 8-12, 2001, AIAA Paper 2001-1031A.
- [50] J. Moss, G. Bird, DSMC Simulations of Hypersonic Flows With Shock Interactions and Validation With Experiments, 37th AIAA Thermophysics Conference, 28 June–1 July, 2004 Portland, OR, AIAA Paper 2004–2585.
- [51] B. Edney, Anomalous heat transfer and pressure distributions on blunt bodies at hypersonic speeds in the presence of an impinging shock, *Flygtekniska Forsoksanstalten* (The Aeronautical Research Institute of Sweden), Stockholm (Rep. 15).
- [52] I. Armenise, M. Capitelli, E. Kustova, E. Nagnibeda, The influence of nonequilibrium kinetics on the heat transfer and diffusion near re-entering body, *J. Thermophys. Heat Transfer* 13 (2) (1999) 210–218.

- [53] I. Armenise, P. Reynier, E. Kustova, Advanced models for vibrational and chemical kinetics applied to Mars entry aerothermodynamics, *J. Thermophys. Heat Transfer* 30 (4) (2016) 705–720.
- [54] A. Kudryavtsev, D. Khotyanovsky, M. Ivanov, A. Hadjadj, D. Vandromme, Numerical investigations of transition between regular and mach reflections caused by free-stream disturbances, *Shock Waves* 12 (2) (2002) 157–165.
- [55] H. Hornung, P. Adam, P. Germain, K. Fujii, A. Rasheed, On transition and transition control in hypervelocity flow, in: *Proceedings of the Ninth Asian Congress of Fluid Mechanics*, 2002.
- [56] D. V. Khotyanovsky, A. N. Kudryavtsev, Numerical simulation of the evolution of unstable disturbances of various modes and initial stages of the laminar-turbulent transition in the boundary layer at the freestream Mach number $M = 6$, *Thermophysics and Aeromechanics* 23 (6) (2016) 809–818.
- [57] G. Markelov, A. Kudryavtsev, M. Ivanov, Continuum and kinetic simulation of laminar separated flow at hypersonic speeds, *Journal of Spacecraft and Rockets* 37 (4) (2000) 499–506.

AppendixA. Grid convergence

A detailed test of grid convergence has been performed for run 1038. The number of grid cells and the corresponding level of grid refinement are given in table A.4. For level 0, a 115×45 grid was used, the height of the first cell from the wedge surface is about 0.5 mm. To evaluate the convergence of the calculation depending on the level of grid refinement, the change in the distribution of the translation-rotational temperature (fig. A.11a-f) and heat flux on the wedge surface (fig. A.12a) was studied. It was obtained that starting from level 4 of grid refinement, the location of the flow separation does not change, but the heat flux downstream still depends on the grid refinement. The dependency of the heat flux on the grid refinement becomes negligible starting from the 5-th level of grid partitioning, and therefore, this grid was used for numerical modeling. The influence of the cell size on the convergence was tested for the first model of vibration-dissociation coupling based on the assumption that computations using the second model would not require additional grid partitioning.

The dependency of the heat flux on the number of iterations is shown on fig. A.12b. We see that on a large region of the wedge surface, the number of iterations does not have an effect on the heat flux, but noticeably affects the main peak of the heat flux on the second wedge's surface. The difference does not exceed 15%. These small differences are due to the long convergence history of the flow in the separation zone and long time for establishing of the final solution.

Table A.4: Grid for run 1038.

grid	level of grid refinement	number of grid cells
level 0	0	5175
level 1	1	12345
level 2	2	38421
level 3	3	133698
level 4	4	499275
level 5	5	1935453
level 6	6	7543245

AppendixB. The influence of chemical reactions and turbulence

In order to understand the role of chemical reactions, we calculate the total heat flux on the body surface without taking into account the dissociation reactions and compare it to previous results.

As was mentioned in the discussion, laminar-turbulent transition can take place in certain zones of the flow. To assess the role of this effect, additional simulations were carried out using the Shear Stress Transport (SST) $k - \omega$ turbulence model with “compressibility effect” and “low-Re correction” options. Turbulent intensity was set at 5%, turbulent length scale was 0.01 m in the free-stream. Additionally, we performed simulation that combined numerical solution of NS equations and Reynolds-averaged NS (RANS) equations. The first part of the flow till the inflection point of the double wedge was calculated using NS equations, while the rest of the computational domain downstream the middle of the double wedge used RANS equations for the computations.

The results of calculations are compared with the experimental data and are presented in the Fig. B.13. Figure B.13a shows the heat flux computed with and without dissociation. We can see a noticeable quantitative discrepancy between the both simulations. Based on comparison with experimental data, we can conclude that taking into account the dissociation reactions is important for correct modeling of the considered flow.

Figure B.13b shows the heat flux computed using the NS equations (“dis, lam” curve) for the whole computational domain, RANS equations (“dis, turb” curve) for the whole computational domain and a combined NS-RANS approach (“dis, lam-turb” curve) which uses NS equations for the flow till the inflection point of the double wedge and RANS equations for the flow downstream the middle of the double wedge.

We see that using the RANS equations in the whole computational domain leads to an overestimation of the heat flux in the region between 10 and 20 mm. The combined NS-RANS approach gives better agreement with the experimental data.

This result is preliminary, however it supports the hypothesis of a laminar-turbulent transitions in local regions of the flow; this should be studied in more

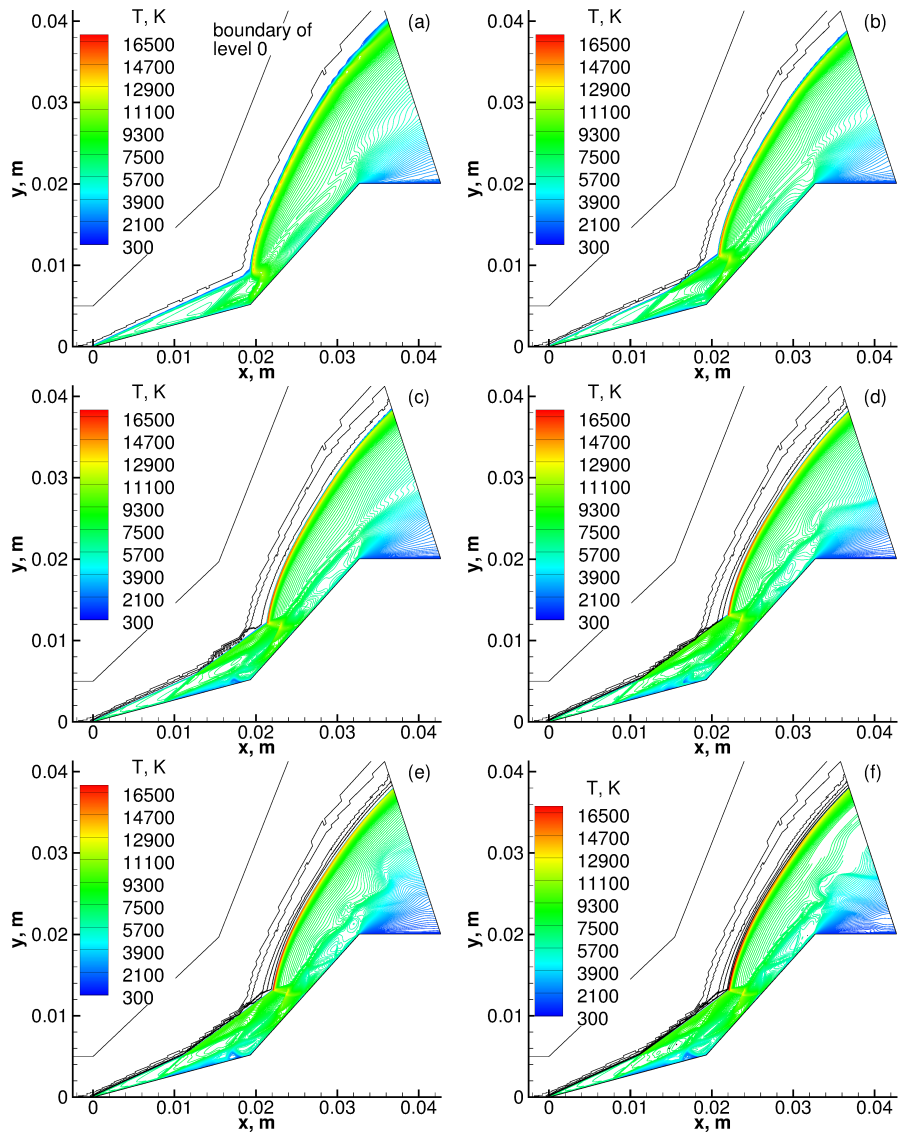


Figure A.11: Grid convergence. Model 1. Case 1038.

detail in the future.

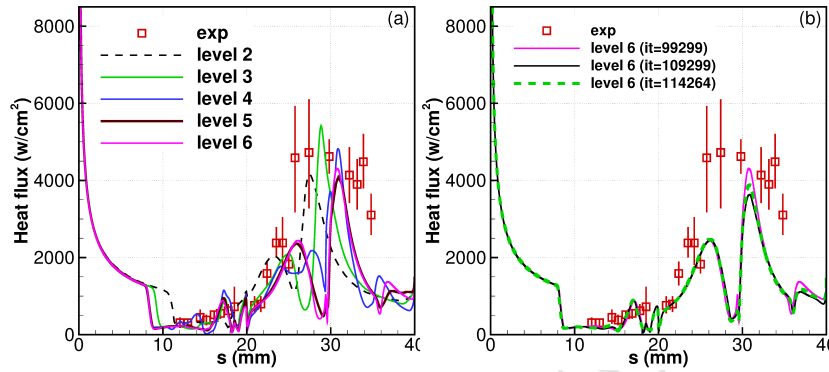


Figure A.12: Heat flux on double wedge surface as a function of cell size (a) and number of iterations (b). Model 1. Case 1038.

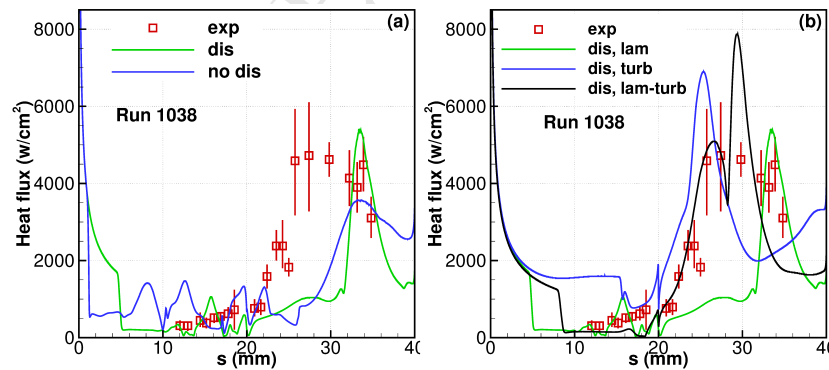


Figure B.13: Effects of chemical reactions (a) and turbulence (b) on the computed heat fluxes on the double wedge surface. Model 2. Case 1038.

1. Recently developed models of vibration-dissociation coupling are validated
2. For high-enthalpy N₂/N flows, new models yield essentially different results
3. Surface heat flux and pressure are in a good agreement with experimental data
4. Different contributions to the heat flux are evaluated